Dalton Transactions

PAPER

View Article Online
View Journal | View Issue

Cite this: *Dalton Trans.*, 2016, **45**, 15541

Triple molybdate scheelite-type upconversion phosphor $NaCaLa(MoO_4)_3:Er^{3+}/Yb^{3+}$: structural and spectroscopic properties†

Chang Sung Lim,[a] Aleksandr S. Aleksandrovsky,[b,c] Maxim S. Molokeev,[d,e] Aleksandr S. Oreshonkov,[f,g] Denis A. Ikonnikov[g] and Victor V. Atuchin*[h,i,j,k]

Received 15th June 2016,
Accepted 24th August 2016

DOI: 10.1039/c6dt02378a

www.rsc.org/dalton

Triple molybdate $NaCaLa_{(1-x-y)}(MoO_4)_3$:$x$Er^{3+},$y$Yb^{3+} ($x = y = 0$, $x = 0.05$ and $y = 0.45$, $x = 0.1$ and $y = 0.2$, $x = 0.2$ and $y = 0$) phosphors were successfully synthesized for the first time by the microwave sol–gel method. Well-crystallized particles formed after heat treatment at 900 °C for 16 h showed a fine and homogeneous morphology with particle sizes of 2–3 μm. The structures were refined by the Rietveld method in the space group $I4_1/a$. The optical properties were examined comparatively using photoluminescence emission and Raman spectroscopy. Under excitation at 980 nm, the $NaCaLa_{0.7}(MoO_4)_3:0.1Er^{3+},0.2Yb^{3+}$ and $NaCaLa_{0.5}(MoO_4)_3:0.05Er^{3+},0.45Yb^{3+}$ particles exhibited a strong 525 nm emission band, a weaker 550 nm emission band in the green region, and three weak 655 nm, 490 nm and 410 nm emission bands in the red, blue and violet regions. The pump power dependence and Commission Internationale de L'Eclairage chromaticity of the upconversion emission intensity were evaluated in detail.

1. Introduction

In recent years, rare-earth doped oxide-based upconversion (UC) particles have become of extensive interest due to their stable luminescent properties and potential applications in photonic products such as lasers, three-dimensional displays, light-emitting devices, solar cells and biological luminescent imaging media.[1–3] Previously, scheelite-type binary molybdates were reported in terms of new structures, including structure-modulation effects, promising spectroscopic characteristics and excellent upconversion (UC) photoluminescence properties.[4–9] In particular, the rare-earth binary $NaLn(MoO_4)_2$ ($Ln = La^{3+}$, Gd^{3+}, Y^{3+}) compounds possess the tetragonal phase with the space group $I4_1/a$, and belong to the family of sheelite-type structures.[10] The trivalent rare-earth ions in the tetragonal phase can be partially substituted by laser-active Er^{3+}, Ho^{3+}, Tm^{3+} and Yb^{3+} ions. These ions are efficiently doped into the crystal lattice of the tetragonal binary molybdates due to the similar radii of the trivalent rare earth ions, which results in the excellent UC photoluminescence properties.[4–9,11–14]

Among rare-earth ions, the Er^{3+} ion is suitable for the infrared to visible light conversion through the UC process due to its appropriate electronic energy level configuration. The Yb^{3+} ion, used as a sensitizer, can be dramatically excited by incident light source energy. This energy is transferred to the activator from which radiation can be emitted. The Er^{3+} ion activator is an efficient luminescence center of the UC particles, while the sensitizer enhances the UC luminescence efficiency. Er^{3+} and Yb^{3+} ion co-doping can remarkably enhance the UC efficiency for the shift from the infrared to visible light due to the efficiency of the energy transfer from Yb^{3+} to Er^{3+}.[15–17]

---

[a] *Department of Advanced Materials Science & Engineering, Hanseo University, Seosan 356-706, Republic of Korea*
[b] *Laboratory of Coherent Optics, Kirensky Institute of Physics, Federal Research Center KSC SB RAS, Krasnoyarsk 660036, Russia*
[c] *Laboratory for Nonlinear Optics and Spectroscopy, Siberian Federal University, Krasnoyarsk 660079, Russia*
[d] *Laboratory of Crystal Physics, Kirensky Institute of Physics, Federal Research Center KSC SB RAS, Krasnoyarsk 660036, Russia*
[e] *Department of Physics, Far Eastern State Transport University, Khabarovsk 680021, Russia*
[f] *Laboratory of Molecular Spectroscopy, Kirensky Institute of Physics, Federal Research Center KSC SB RAS, Krasnoyarsk 660036, Russia*
[g] *Department of Photonics and Laser Technologies, Siberian Federal University, Krasnoyarsk 660079, Russia*
[h] *Laboratory of Optical Materials and Structures, Institute of Semiconductor Physics, SB RAS, Novosibirsk 630090, Russia. E-mail: atuchin@isp.nsc.ru; Fax: +7 (383) 3332771; Tel: +7 (383) 3308889*
[i] *Functional Electronics Laboratory, Tomsk State University, Tomsk 634050, Russia*
[j] *Laboratory of Semiconductor and Dielectric Materials, Novosibirsk State University, Novosibirsk 630090, Russia*
[k] *Institute of Chemistry, Tyumen State University, Tyumen 525003, Russia*

† Electronic supplementary information (ESI) available. See DOI: 10.1039/c6dt02378a

For the preparation of the double molybdate $NaLn(MoO_4)_2$, several processes have been developed *via* specific preparation processes, including solid-state reactions,[4,8,18–21] the sol–gel method,[22,23] Czochralski growth,[24–27] the hydrothermal method,[28–32] the microwave assisted hydrothermal method[33] and pulsed laser deposition.[34] Nevertheless, it is necessary to create new triple molybdate compounds for the observation of the UC photoluminescence in the materials and to search for features such as a well-defined morphology and stable UC luminescent properties. However, so far, triple molybdates with the general composition $NaRLn(MoO_4)_3$ ($R = Ca^{2+}$, Sr^{2+} and Ba^{2+}, while Ln is a rare-earth element) have not been reported. Compared to the common technological methods, microwave synthesis has its advantages of a very short reaction time, small particle size, narrow particle size distribution, and high final polycrystalline sample purity.[35,36] The microwave heating is delivered to the material surface by radiant and/or convection heating and the heat energy is transferred to the bulk of the material *via* conduction.[37–39] It is an inexpensive method that provides high-homogeneity powder products and it is easy to scale up the process. Thus, the microwave method is considered a viable alternative approach for the quick synthesis of high-quality luminescent materials. In this concept, this method is optimal for the synthesis of complex oxide compounds.

In the present study, triple molybdate $NaCaLa_{(1-x-y)}(MoO_4)_3{:}xEr^{3+},yYb^{3+}$ ($NCLM{:}xEr^{3+},yYb^{3+}$) phosphors with correct doping concentrations of Er^{3+} and Yb^{3+} ($x = y = 0$, $x = 0.05$ and $y = 0.45$, $x = 0.1$ and $y = 0.2$, $x = 0.2$ and $y = 0$) were successfully prepared by the microwave sol–gel method followed by heat treatment in air. The synthesized particles were characterized by X-ray diffraction (XRD), scanning electron microscopy (SEM) and energy-dispersive X-ray spectroscopy (EDS). Their optical properties were examined comparatively using photoluminescence (PL) emission and Raman spectroscopy. The pump power dependence and Commission Internationale de L'Eclairage (CIE) chromaticity parameters of the UC emission were evaluated in detail.

2. Experimental methods

In this study, precise amounts of the raw materials, the products of Sigma-Aldrich (USA) for $Ca(NO_3)_2{\cdot}4H_2O$ (99%), $Na_2MoO_4{\cdot}2H_2O$ (99%), $La(NO_3)_3{\cdot}6H_2O$ (99%), $Er(NO_3)_3{\cdot}5H_2O$ (99.9%), $Yb(NO_3)_3{\cdot}5H_2O$ (99.9%), Alfa Aesar (USA) for $(NH_4)_6Mo_7O_{24}{\cdot}4H_2O$ (99%), Daejung Chemicals (Korea) for citric acid (99.5%), $NH_3{\cdot}H_2O$ (A.R.), ethylene glycol (A.R.) and distilled water, were used to prepare $NaCaLa(MoO_4)_3$, $NaCaLa_{0.8}(MoO_4)_3{:}0.2Er^{3+}$, $NaCaLa_{0.7}(MoO_4)_3{:}0.1Er^{3+},0.2Yb^{3+}$, and $NaCaLa_{0.5}(MoO_4)_3{:}0.05Er^{3+},0.45Yb^{3+}$ compositions. The reagents were taken in accordance with the nominal composition of the designed compounds. For the preparation of the compounds, initially 0.4 mol% $Ca(NO_3)_2$, 0.2 mol% $Na_2MoO_4{\cdot}2H_2O$ and 0.143 mol% $(NH_4)_6Mo_7O_{24}{\cdot}4H_2O$ were dissolved in 20 mL of ethylene glycol and 80 mL of 5 M $NH_3{\cdot}H_2O$ under vigorous stirring and heating. Subsequently, 0.4 mol% $(1-x-y)La(NO_3)_3{\cdot}6H_2O$ with 0.4 mol% $xEr(NO_3)_3{\cdot}5H_2O$ and 0.4 mol% $yYb(NO_3)_3{\cdot}5H_2O$ ($x = 0.05$ and $y = 0.45$, $x = 0.1$ and $y = 0.2$, $x = 0.2$ and $y = 0$) were dissolved in 100 mL of distilled water under vigorous stirring and heating. At this stage, citric acid was employed with the molar ratio of citric acid to metal ions of 2 : 1. Then, the two kinds of transparent solutions were co-mixed together under vigorous stirring under heating at 80–100 °C. Finally, the mixed solutions appeared highly transparent and were treated by adjusting to pH = 7–8 using the addition of citric acid or $NH_3{\cdot}H_2O$. The co-mixed and adjusted solutions were transferred into an oven for microwave irradiation. Microwave operations for 30 min were conducted by precise controlling. The frequency was 2.45 GHz and the maximum output-power was 1250 W. After the microwave process, the samples were treated in an ultrasonicator for 10 min, and transferred into a dry oven. The drying conditions were at 120 °C and dried gels in black color were obtained. For the crystallization of the compounds, the black dried gels were heat-treated at 900 °C for 16 h. Finally, white pure $NaCaLa(MoO_4)_3$ and pink particles for the Er/Yb-doped compositions were obtained. The chemical compositions of the final powder products were confirmed using EDS measurements.

The powder diffraction data of the synthesized particles for Rietveld analysis were collected over the range of $2\theta = 5$–$90°$ at room temperature with a D/MAX 2200 (Rigaku, Japan) diffractometer (Cu-Kα radiation, θ–2θ geometry). The step size of 2θ was 0.02°, and the counting time was 5 s per step. The microstructure and surface morphology of the synthesized particles were examined using SEM (JSM-5600, JEOL, Japan). PL spectra were recorded using a spectrophotometer (Perkin Elmer LS55, UK) at room temperature. The pump power dependence of the UC emission intensity was measured at working power from 20 to 110 mW levels. Raman spectroscopy measurements were performed using a LabRam Aramis (Horiba Jobin-Yvon, France) with the spectral resolution of 2 cm^{-1}. The 514.5 nm line of an Ar ion laser was used as an excitation source; the power on the samples was kept at the 0.5 mW level to avoid decomposition of the sample.

3. Results and discussion

The XRD patterns recorded from the synthesized molybdates are shown in Fig. 1 and 1S–3S.† In general, the patterns of solutions $NCLM{:}xEr^{3+},yYb^{3+}$ are similar. The difference profile plot of NCLM is shown in Fig. 1. The difference profile plots of $NCLM{:}xEr^{3+},yYb^{3}$ are very similar to that of NCLM, as is evident from a comparison of Fig. 1 and 1S–3S.†

Rietveld refinement was performed using the TOPAS 4.2 package.[40] All diffraction peaks were indexed using the tetragonal unit cell in the space group $I4_1/a$ with parameters close to those of $CaMoO_4$ [41] and $Na_{0.5}La_{0.5}MoO_4$.[42] Therefore, these crystal structures were taken as a starting model for the Rietveld refinement. The site of the Ca or (Na/La) ion was taken as occupied by Ca, Na, La, Er, and Yb ions at fixed

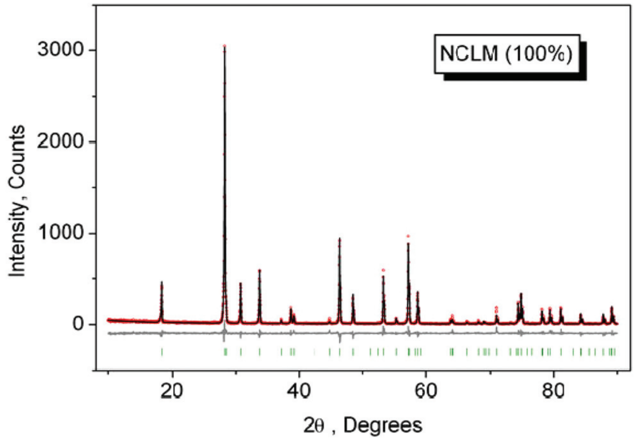

Fig. 1 The difference Rietveld plot of NCLM.

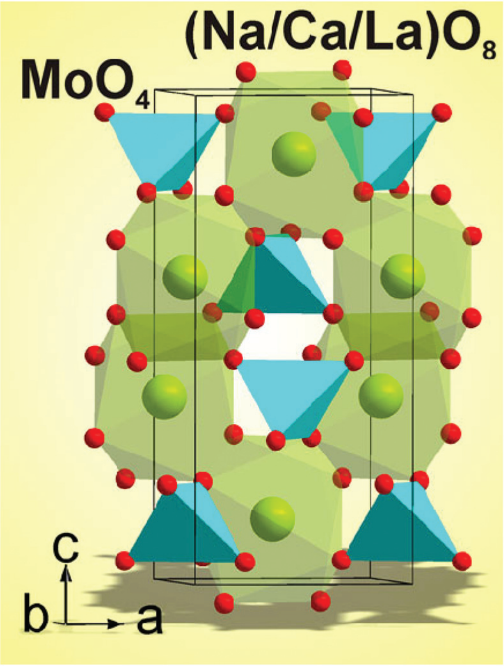

Fig. 2 The crystal structure of NCLM. The unit cell is outlined.

occupations according to the nominal compositions. The refinement was stable and gave low *R*-factors (Table 1, Fig. 1 and 1S–3S†). The obtained atomic coordinates and the main bond lengths can be found in Tables 1S and 2S,† respectively. In the compounds under consideration, $Z = 4$ and, from the structural point of view,[43] the total chemical formula calculated by summing all elements in the unit cell $Na_{4/3}Ca_{4/3}La_{4(1-x-y)/3}(MoO_4)_4{:}4x/3Er^{3+},4y/3Yb^{3+}$ can be generalized as $Na_{1/3}Ca_{1/3}La_{(1-x-y)/3}MoO_4{:}(x/3)Er^{3+},(y/3)Yb^{3+}$, which clearly emphasizes the relationship of the solid solutions to the $CaMoO_4$ structural family.[41] As an example, the structure of NCLM is shown in Fig. 2.

The linear cell volume increase with the averaged increase of ion radii IR(Na/Ca/La/Er/Yb), as shown in Fig. 3, proves the chemical compositions of the synthesized samples.[44] On the basis of the structural results, it can be reasonably supposed that different triple molybdates with the general composition $NaRLn(MoO_4)_3$ should crystallize in tetragonal structures close to that of $CaMoO_4$ and the general formula should be rewritten as $Na_{1/3}R_{1/3}Ln_{1/3}MoO_4$. Further details of the crystal structure may be obtained from Fachinformationszentrum Karlsruhe, 76344 Eggenstein-Leopoldshafen, Germany (fax: (+49)7247-808-666; e-mail: crystdata@fiz-karlsruhe.de; http://www.fiz-karlsruhe.de/request_for_deposited_data.html) on quoting the deposition numbers: CSD 431015–431018.

Thus, post heat-treatment plays an important role in molybdate gel crystallization. To reach a high-quality crystalline state, samples need to be heat treated at 900 °C for 16 h. It should be pointed out that this temperature is optimal for molybdate treatment in air and, earlier, other simple and complex molybdates were formed at close temperatures.[6,7,9,37–39,45–47] Besides excellent crystallinity, the selected synthesis route provides a uniform particle morphology. The SEM images of the synthesized (a) NCLM:0.2Er^{3+} and (b) NCLM:0.05Er^{3+},0.45Yb^{3+} particles are shown in Fig. 4.

Table 1 Main parameters of the processing and refinement of the NCLM:xEr^{3+},yYb^{3+} samples

Compound	NCLM	NCLM:0.2Er^{3+}	NCLM:0.1Er^{3+},0.2Yb^{3+}	NCLM:0.05Er^{3+},0.45Yb^{3+}
x	0	0.2	0.1	0.05
y	0	0	0.2	0.45
Sp. gr.	$I4_1/a$	$I4_1/a$	$I4_1/a$	$I4_1/a$
a, Å	5.2991 (1)	5.2806 (2)	5.2675 (1)	5.2421 (1)
c, Å	11.6223 (3)	11.5726 (3)	11.5377 (3)	11.4678 (2)
V, Å^3	326.37 (2)	322.70 (1)	320.13 (2)	315.17 (1)
Z	4	4	4	4
2θ-interval, °	5–90	5–90	5–90	5–90
No. of reflections	70	70	70	70
No. of refined parameters	7	7	7	7
R_{wp}, %	19.46	16.75	15.65	15.06
R_p, %	13.39	11.30	10.31	9.97
R_{exp}, %	16.22	14.87	13.61	13.49
χ^2	1.20	1.13	1.15	1.12
R_B, %	5.29	3.15	2.09	1.65

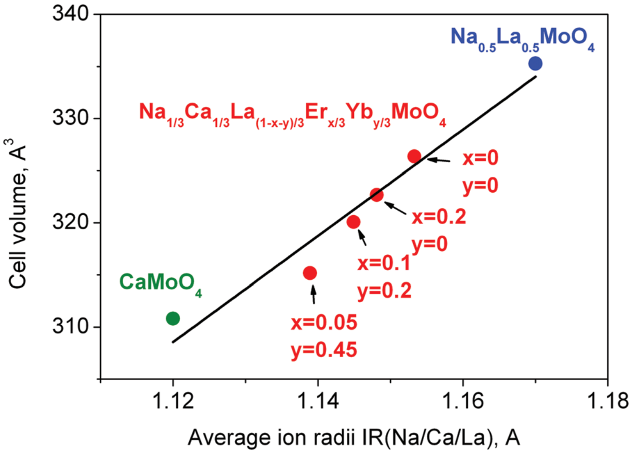

Fig. 3 Cell volume per averaged ion radii IR(Na/Ca/La/Er/Yb) of $CaMoO_4$ (green),[41] NCLM:xEr^{3+},yYb^{3+} (red) and $Na_{0.5}La_{0.5}MoO_4$ (blue)[42] compounds.

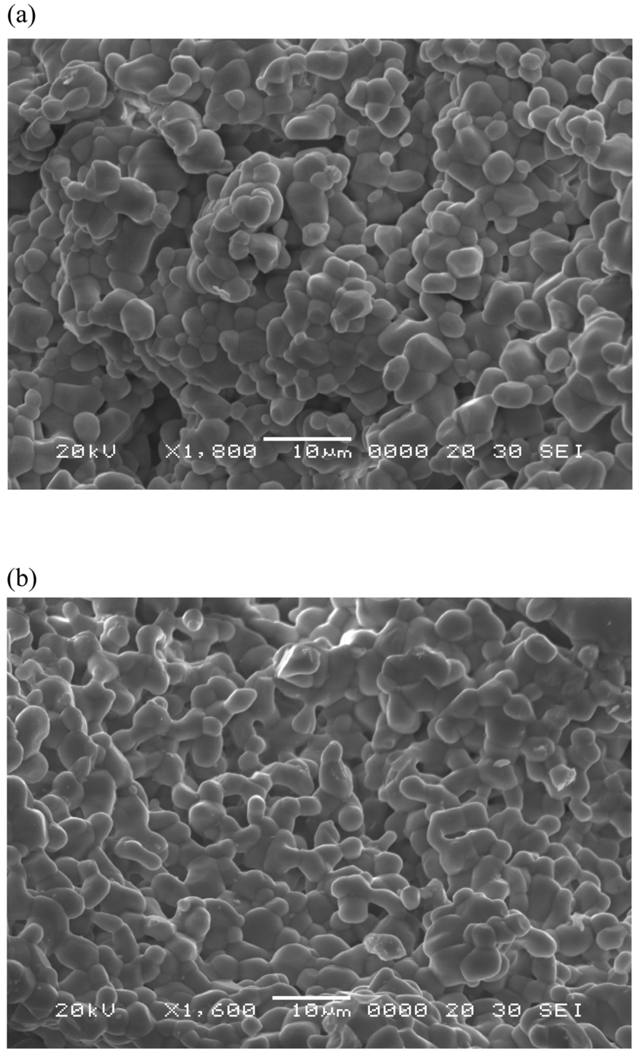

Fig. 4 Scanning electron microscopy images of the synthesized (a) NCLM:0.2Er^{3+} and (b) NCLM:0.05Er^{3+},0.45Yb^{3+} particles.

The as-synthesized samples are well formed with a fine and homogeneous morphology and a particle size of 2–3 μm. The samples show no discrepancy in the aspect of morphological features, and closely agglomerated particles were induced by active grain interdiffusion.[48–50] It should be noted that doping concentrations of Er^{3+} and Yb^{3+} have no effects on the particle morphology. The recorded EDS patterns and quantitative compositions of the NCLM:0.1Er^{3+},0.2Yb^{3+} sample are shown in Fig. 4S and Table 3S.† Only constituent elements are found in the samples and the quantitative compositions are in good accord with nominal compositions. Thus, the microwave sol–gel method of triple molybdate preparation provides energy uniformly over the material bulk, and fine particles with controlled morphology can be fabricated in a short time. The method is an inexpensive way to fabricate highly homogeneous powder products with an easy scale-up and is a viable alternative for the rapid synthesis of UC particles. This suggests that the microwave sol–gel route is suitable for the creation of homogeneous NCLM:xEr^{3+},yYb^{3+} crystallites and can be successfully applied to other molybdates from this crystal family.

The UC photoluminescence emission spectra of the as-prepared NCLM, NCLM:0.2Er^{3+}, NCLM:0.1Er^{3+},0.2Yb^{3+} and NCLM:0.05Er^{3+},0.45Yb^{3+} particles excited at 980 nm at room temperature are shown in Fig. 5. The UC NCLM:0.1Er^{3+},0.2Yb^{3+} and NCLM:0.05Er^{3+},0.45Yb^{3+} particles exhibited a strong 525 nm emission band, a weaker 550 nm emission band in the green region and three very weak emission bands: at 655 nm in the red region, at 490 nm in the blue region, and at 410 nm in the violet region. The strong 525 nm emission band and the weak 550 nm emission band in the green region correspond to the $^2H_{11/2} \rightarrow {}^4I_{15/2}$ and $^4S_{3/2} \rightarrow {}^4I_{15/2}$ transitions, respectively, while the very weak 655 nm emission band in the red region corresponds to the $^4F_{9/2} \rightarrow {}^4I_{15/2}$ transition. Another very weak band at 410 nm is due to the $^2H_{9/2} \rightarrow {}^4I_{15/2}$ transition, while a

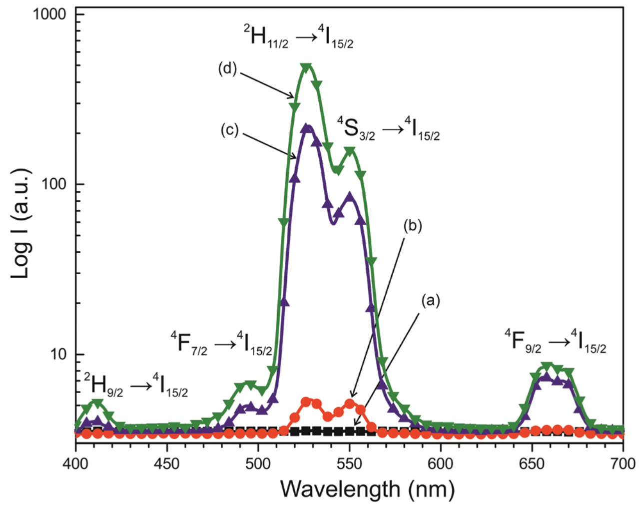

Fig. 5 The upconversion photoluminescence emission spectra of (a) NCLM, (b) NCLM:0.2Er^{3+}, (c) NCLM:0.1Er^{3+},0.2Yb^{3+}, and (d) NCLM:0.05Er^{3+},0.45Yb^{3+} particles excited at 980 nm at room temperature. The logarithmic scale is used along the vertical axis.

490 nm peak is due to the $^4F_{9/2} \rightarrow {}^4I_{15/2}$ transition. It must be noted that in sample (d), the shortest-wavelength band at 410 nm is only two times smaller than the red one, despite the fact that a three-stage process is necessary to excite the $^2H_{9/2}$ level. The mechanism of excitation of this level might be the energy transfer from the Yb excited state to the Er $^4F_{9/2}$ level, since the energy difference between $^4F_{9/2}$ and $^2H_{9/2}$ is close to the energy of the excited Yb ion. However, since the $^4F_{9/2}$ population is likely to be low, the most probable excitation channel is the population of a pair of high-lying levels $^4G_{9/2}$ and $^2K_{15/2}$ from the well-populated $^4S_{3/2}$ level through the energy transfer from the Yb ion, with the subsequent decay of these high-lying levels to the $^2H_{9/2}$ one.

The UC intensities of NCLM were not detected. The UC intensities of NCLM:0.2Er^{3+} are well above the detection limit; however, they are one or two orders of magnitude smaller than those of the Yb-doped samples and, hence, the UC luminescence for an Er-doped sample is not well seen in Fig. 5. The UC luminescence is observed from all levels: $^2H_{11/2}$, $^4S_{3/2}$ and even from $^4F_{9/2}$. The intensity ratio of green and red lines is 1.4 for sample (b), 30 for sample (c) and 56 for sample (d). At the same time, the ratio of UC green band peak values for samples (d) and (b) is 92. The latter effect admits that the absorption coefficient of erbium at 980 nm is much smaller than that of ytterbium in the matrix under study. The variation of the green-to-red ratio with the ytterbium content increase is rather common and was observed earlier for several hosts.[15–17,37–39]

The Er^{3+} ion activator is the luminescence center of these UC particles and the sensitizer Yb^{3+} effectively enhances the UC luminescence intensity because of efficient energy transfer from Yb^{3+} to Er^{3+}. The concentration quenching effect can be explained by the energy transfer between the nearest Er^{3+} and Yb^{3+} ions. On increasing the Er^{3+} and Yb^{3+} ion concentrations, the distance between Er^{3+} and Yb^{3+} ions decreases, which can promote a non-radiative energy transfer, such as an exchange interaction or multipole–multipole interactions.[51] As shown in Fig. 5, the higher intensity of (d) NCLM:0.05Er^{3+},0.45Yb^{3+} is caused by the ratio of Yb^{3+} : Er^{3+} = 9 : 1, while the lower intensity of (c) NCLM:0.1Er^{3+},0.2Yb^{3+} is caused by the ratio of Yb^{3+} : Er^{3+} = 2 : 1. Thus, the preferable Yb^{3+} : Er^{3+} = 9 : 1 ratio is induced by the concentration quenching effect of Er^{3+} ions. Therefore, the higher content of the Yb^{3+} ions used as a sensitizer and the lower content of the Er^{3+} ions close to the preferable ratio of Yb^{3+} : Er^{3+} = 9 : 1 can remarkably enhance the UC luminescence through the efficient energy transfer. The ratio of the $^2H_{11/2} \rightarrow {}^4I_{15/2}$ and $^4S_{3/2} \rightarrow {}^4I_{15/2}$ transition intensities may be influenced not only by the change in radiation probabilities from starting levels, but also by the probabilities of the non-radiative relaxation from the UC-populated $^4F_{7/2}$ level. Because the lifetime of the $^4F_{7/2}$ level is comparatively short, the excited Er^{3+} ions decay non-radiatively to the $^2H_{11/2}$ level with a higher probability, as compared to the $^4S_{3/2}$ level, in the case of the NCLM host matrix.

The logarithmic scale dependences of the UC emission intensities at 525, 550 and 655 nm on the working pump power over the range of 20–110 mW in the NCLM:0.05Er^{3+},0.45Yb^{3+} sample are shown in Fig. 6. In the UC process, the UC emission intensity I is proportional to the slope value n of the irradiation pumping power P. The maximum value of n is the number of pumping photons required to reach the starting energy level in the UC ion and produce UC emission:[52]

$$I \propto P^n \tag{1}$$

$$\ln I \propto n \ln P \tag{2}$$

The slopes n = 1.70 and 1.68 for green emission at 525 and 550 nm, and n = 1.56 for red emission at 655 nm, respectively, are evident from Fig. 5. These results show that the UC mechanism of the green and red emissions can be explained by a two-photon UC process in the Er^{3+}/Yb^{3+} co-doped phosphors.[53–55]

Based on the results of the analysis of pump power dependence, the schematic energy level diagrams of Er^{3+} ions (activator) and Yb^{3+} ions (sensitizer) in the NCLM:xEr^{3+},yYb^{3+} samples and the UC mechanisms, accounting for the green and red emissions excited by the 980 nm laser wavelength, are shown in Fig. 7. The UC emissions are generated *via* multiple processes of ground state absorption (GSA), energy transfer upconversion (ETU), excited state absorption (ESA) and cross relaxation (CR). Under excitation at 980 nm, the Er^{3+} and Yb^{3+} ions are initially excited from the ground state to the excited state through the ground state absorption (GSA) process (Er^{3+}: $^4I_{15/2} \rightarrow {}^4I_{11/2}$, Yb^{3+}: $^2F_{7/2} \rightarrow {}^2F_{5/2}$) and ETU processes of $^4I_{15/2}$ (Er^{3+}) + $^2F_{5/2}$ (Yb^{3+}) → $^4I_{11/2}$ (Er^{3+}) + $^2F_{7/2}$ (Yb^{3+}), which are responsible for the population at the $^4I_{11/2}$ level in the Er^{3+} ion. For the green emissions, the energy transition from the $^4I_{11/2}$ level to the $^4F_{7/2}$ level of Er^{3+} is involved in three possible processes:[53–55] (1) ESA: $^4I_{11/2}$ (Er^{3+}) + a photon (980 nm) → $^4F_{7/2}$, (2) ETU: $^2I_{11/2}$ (Er^{3+}) + $^2F_{5/2}$ (Yb^{3+}) → $^4F_{7/2}$ (Er^{3+}) + $^2F_{7/2}$ (Yb^{3+}) and (3) ETU: $^4I_{11/2}$ (Er^{3+}) + $^4I_{11/2}$ (Er^{3+}) → $^4F_{7/2}$ (Er^{3+}) + $^4I_{15/2}$

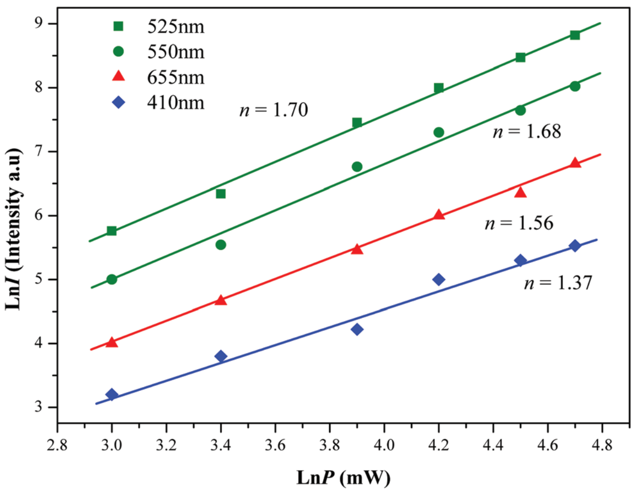

Fig. 6 The logarithmic scale dependence of the upconversion emission intensity on the pump power in the range of 20–110 mW at 525, 550, 655 and 410 nm in the NCLM:0.05Er^{3+},0.45Yb^{3+} sample.

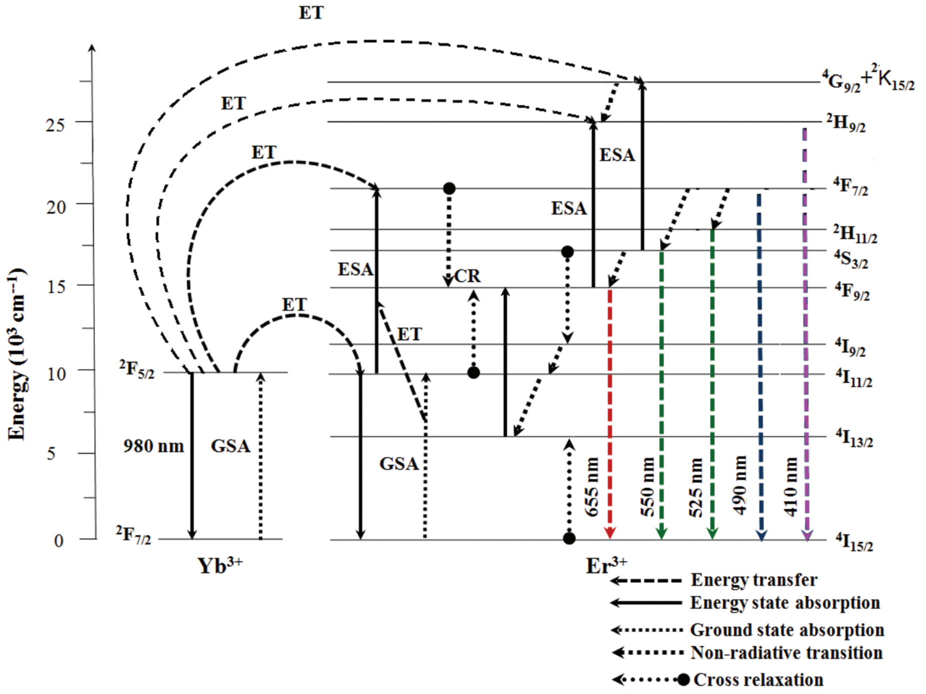

Fig. 7 The schematic energy level diagrams of Yb^{3+} (sensitizer) and Er^{3+} ions (activator) in the NCLM:xEr^{3+},yYb^{3+} system and the upconversion mechanisms of the green and red emissions under 980 nm laser excitation.

(Er^{3+}). These three possible processes can populate the $^4F_{7/2}$ level from the $^4I_{11/2}$ level in Er^{3+} and, then, the $^4F_{7/2}$ level relaxes rapidly and non-radiatively to the next lower $^2H_{11/2}$ and $^4S_{3/2}$ levels in Er^{3+} because of the short lifetime of the $^4F_{7/2}$ level. As a result, the radiative transitions of $^2H_{11/2} \rightarrow {}^4I_{15/2}$ and $^4S_{3/2} \rightarrow {}^4I_{15/2}$ processes can generate the green emission at 525 and 550 nm. The strong suppression of red UC luminescence in the host under study is similar to the effect in the earlier studied $CaGd_2(MoO_4)_4$:Er,Yb and $CaGd_2(WO_4)_4$:Er,Yb systems and differentiates this host class from a number of others. For the red emission, the $^4F_{9/2}$ level population is generated by non-radiative relaxation either (1) from the $^4S_{3/2}$ to the $^4F_{9/2}$ level or (2) from $I_{11/2}$ to $I_{13/2}$, and then pumping to $^4F_{9/2}$, as well as by cross relaxation (CR) *via* either (3) the $^4F_{7/2} + {}^4I_{11/2} \rightarrow {}^4F_{9/2} + {}^4F_{9/2}$ transition[51–53] or (4) $^4S_{3/2} + {}^4I_{15/2} = {}^4I_{9/2} + {}^4I_{13/2}$, and then pumping to $^4F_{9/2}$.[56] Finally, the $^4F_{9/2}$ level relaxes radiatively to the ground state at the $^4I_{15/2}$ level, and releases the red emission at 655 nm.[37–39] The radiation-free transitions (1) and (2) must not strongly vary from one oxide host to another and, then, they cannot provide such a significant difference between the red and green luminescence in the selected group of hosts. Consequently, processes (1) and (2) must be deduced to play a negligible role in the host class under study. So, intense red luminescence at the Er/Yb ratio of 3/8 is most likely, due to one of the mentioned cross-relaxation channels.[54] The (3) $^4F_{7/2} + {}^4I_{11/2} = {}^4F_{9/2} + {}^4F_{9/2}$ cross-relaxation will be very weak since $^4F_{7/2}$ has a comparatively short lifetime and its radiationless depopulation to $^4S_{3/2}$ and $^2H_{11/2}$ levels is rather fast, which may explain the weak red luminescence in our host. For the (4) population channel, the weak red UC luminescence is explainable by the suggestion that, in our host, detuning between the energy of the $^4S_{3/2}$ state and the sum of the energies of $^4I_{9/2}$ and $^4I_{13/2}$ states is not so favorable.[54] Moreover, as Yb^{3+} concentration increases, the green emission dramatically increases, compared to the red emission. The strong 525 nm and 550 nm emission lines in the green region, as shown in Fig. 5, are assigned to the $^2H_{11/2} \rightarrow {}^4I_{15/2}$ and $^4S_{3/2} \rightarrow {}^4I_{15/2}$ transitions of the Er^{3+} ions, respectively, while the weak 655 nm emission band in the red region is assigned to the $^4F_{9/2} \rightarrow {}^4I_{15/2}$ transition.

The chromaticity coordinates calculated for (a) NCLM:$0.1Er^{3+}$,$0.2Yb^{3+}$ and (b) NCLM:$0.05Er^{3+}$,$0.45Yb^{3+}$ particles and the related CIE chromaticity diagram are shown in Fig. 8. The legend of Fig. 8(B) shows the chromaticity points for samples (a) and (b). When the Er^{3+}/Yb^{3+} concentration ratio is varied, the chromaticity coordinate values (x, y) change. As shown in Fig. 8(A), the calculated chromaticity coordinates $x = 0.227$ and $y = 0.686$ for (a) NCLM:$0.1Er^{3+}$,$0.2Yb^{3+}$ and $x = 0.206$ and $y = 0.727$ for (b) NCLM:$0.05Er^{3+}$,$0.45Yb^{3+}$ correspond to the yellowish-green sector in the CIE diagram.

The Raman spectra of the synthesized pure NCLM, NCLM:$0.2Er^{3+}$, NCLM:$0.1Er^{3+}$,$0.2Yb^{3+}$ and NCLM:$0.05Er^{3+}$,$0.45Yb^{3+}$ particles are shown in Fig. 9. As to pure NCLM, the well-resolved sharp peaks clearly indicate a highly crystalline state of the synthesized particles. The symmetry and frequencies of all the observed modes in the Raman spectrum of pure NCLM in comparison with the Raman spectrum of isostructural $CaMoO_4$[57,58] are presented in Table 2. The decomposition of spectral regions corresponding to the bending and stretching vibrations of MoO_4 tetrahedra is shown in Fig. 10.

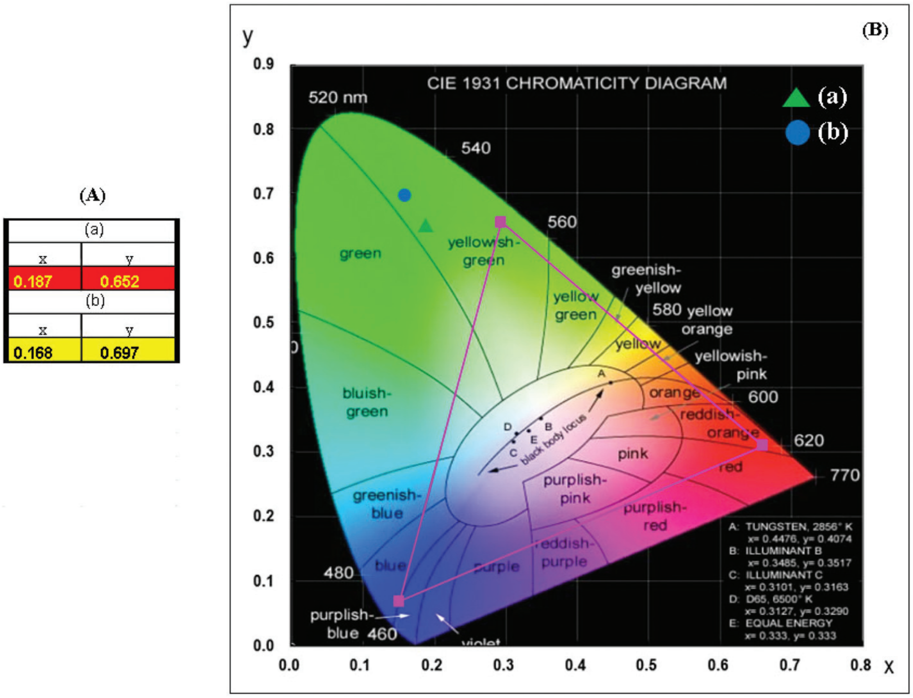

(A)

(a)	
x	y
0.187	0.652
(b)	
x	y
0.168	0.697

Fig. 8 (A) Calculated chromaticity coordinate (*x*, *y*) values and (B) the CIE chromaticity diagram for the NCLM:$x\mathrm{Er}^{3+}$,$y\mathrm{Yb}^{3+}$ phosphors. The emission points for the sample (a) NCLM:0.1Er^{3+},0.2Yb^{3+} and (b) NCLM:0.05Er^{3+},0.45Yb^{3+} particles are shown in the inset.

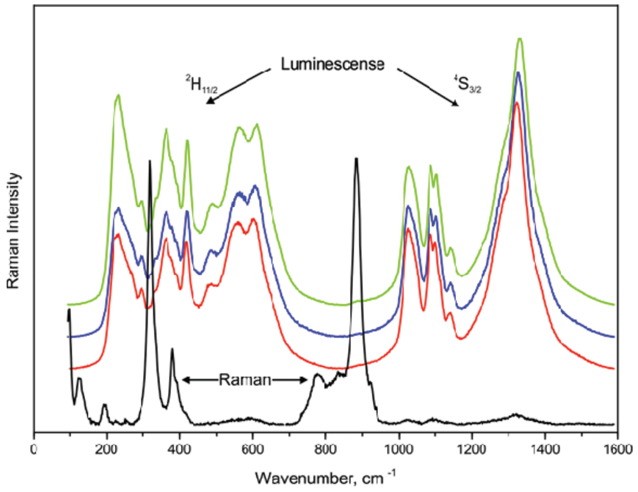

Fig. 9 Emission (Raman and luminescence) spectra of the synthesized (black) NCLM, (red) NCLM:0.2Er^{3+}, (blue) NCLM:0.1Er^{3+},0.2Yb^{3+}, and (green) NCLM:0.05Er^{3+},0.45Yb^{3+} particles excited by the 514.5 nm line of an Ar ion laser at 0.5 mW. Luminescence from $^2\mathrm{H}_{11/2}$ and $^4\mathrm{S}_{3/2}$ multiplets of the Er^{3+} ion is indicated.

To perform the lattice dynamics (LD) simulation of the investigated compounds, the program package LADY was used.[59] The atomic vibration frequencies were obtained using a modified random-element-isodisplacement model.[60] Only the pair-wise interactions and bond-stretching force constants *A* are considered. *A* depends on r_{ij}, and the $A(r_{ij})$ dependences are the same for all atom pairs – $A = \lambda \exp(-r_{ij}/\rho)$, where r_{ij} is the interatomic distance, and λ and ρ are the parameters characterizing the selected pair interaction. To find model parameters, a special optimization program was written and tested for several compounds from different chemical classes.[7,47,61–66] The initial parameter values were accepted as random ones and lattice stability conditions were taken into account. The resulting model parameters were obtained by minimization of residual difference values of the simulated and experimental Raman frequencies of pure NCLM using the Fletcher–Reeves method.[67] In the case of suspension of the Fletcher–Reeves algorithm because of incompatible model parameters, the initial model parameters were set randomly again. To obtain a satisfactory agreement between experimental and calculated results, O–O interatomic interactions within MoO_4 tetrahedral groups and O–O intermolecular interactions between neighboring MoO_4 groups should be described within different force constants, and the cation–cation interactions can be neglected.[68,69] The model parameters obtained for pure NCLM are shown in Table 4S.† The simulations of NCLM:0.2Er^{3+}, NCLM:0.1Er^{3+},0.2Yb^{3+}, and NCLM:0.05Er^{3+},0.45Yb^{3+} were carried out using the same model parameters. Uniform values of Er–O, Yb–O and La–O force constants were selected. A comparison of the observed and calculated Raman modes of pure NCLM can be found in Table 2. Calculations predict noticeable shifts of Raman frequencies in doped samples; the extent of these shifts is in general agreement with the variation of Mo–O length according to the empirical formula of Hardcastle.[70] However, the

Table 2 Notation and wavenumber values (cm^{-1}) of the active Raman lines in (a) NCLM, (b) NCLM:$0.2Er^{3+}$, (c) NCLM:$0.1Er^{3+}$,$0.2Yb^{3+}$ and (d) NCLM:$0.05Er^{3+}$,$0.45Yb^{3+}$

			Calc.				Exp.	
Number	Symmetry type	Exp. (a)		(b)	(c)	(d)	$CaMoO_4$ [57,58]	$CaLa_2(MoO_4)_4$ [7]
1	A_g	885	881	907	874	895	877	906
2	B_g	829	822	849	826	841	845	828
3	E_g	777	785	804	779	798	792	762
4	B_g	390	398	420	424	430	402	393
5	E_g	380	371	378	384	388	391	377
6	B_g	332	330	328	315	328	327	333
7	A_g	318	326	348	343	347	321	317
8	E_g	255	241	257	267	272	267	251
9	B_g	228	231	219	229	229	214	
10	A_g	195	202	193	200	202	204	193
11	E_g	190	183	186	192	196	189	
12	B_g	141	142	149	151	152	143	
13	E_g	125	127	131	134	137	111	
14	B_g	96	96	90	95	95		
15	E_g		79	80	83	85		
16	B_g		21	20	21.4	21.4		
17	E_g		18	18	18.8	19.4		
18	B_g			18	19.7	19.6		
19	E_g			16	17.2	17.7		
20	B_g				19.1	19.1		
21	E_g				16.8	17.4		

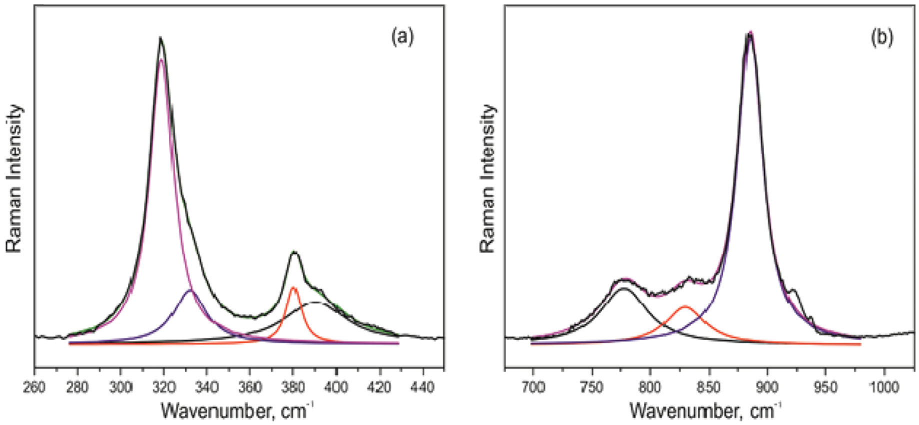

Fig. 10 The decomposition of Raman spectra of NCLM in the regions of (a) bending and (b) stretching vibrations of MoO_4 tetrahedra.

Raman signals measured for Er-doped compositions cannot be directly compared to the simulated results because of strong Er^{3+} luminescence, and the experimental check will be the subject of a separate study.

By the group theory analysis, 17 active Raman modes were predicted for the NCLM structure: $\Gamma_{raman} = 3A_g + 7B_g + 7E_g$; 19 active modes for NCLM:$0.2Er^{3+}$: $\Gamma_{raman} = 3A_g + 8B_g + 8E_g$; 21 active modes for NCLM:$0.1Er^{3+}$,$0.2Yb^{3+}$ and NCLM:$0.05Er^{3+}$,$0.45Yb^{3+}$: $\Gamma_{raman} = 3A_g + 9B_g + 9E_g$. As can be seen from Table 2, additional modes, in comparison with pure molybdate, should be observed in the Raman spectra of Er,Y-doped compounds in the range below 80 cm^{-1}. The most intensive band of the NCLM Raman spectrum found at 884 cm^{-1} corresponds to the ν_1 symmetric stretching vibration of the MoO_4 group. The lines at 829 and 777 cm^{-1} are related to the ν_3 antisymmetric stretching vibrations. The bending ν_2 and ν_4 vibrations are situated in the wavenumber region of 300–400 cm^{-1}. The shape of the observed normal vibration modes of tetrahedral MoO_4 groups has been considered in ref. 71. The translation and rotational vibrations of MoO_4 are in the region of 150–260 cm^{-1}. The big cation vibrations are below 150 cm^{-1}. As can be seen from a comparison of Raman spectra of pure NCLM and $CaLa_2(MoO_4)_4$[7] shown in Fig. 5S,† the positions of the bands corresponding to the symmetric stretching of MoO_4 are slightly different in these crystals. In this case, according to the LD model presented above, Mo–O bonds should have different lengths in these molybdates and this is confirmed by structural results (Table 2S†). As to Raman spectra of the doped samples recorded under excitation at 514.5 nm, the Raman lines are superimposed by strong Er^{3+} luminescence lines. To consider the vibrational spectra of these samples, it is topical to use an excitation source with a drastically longer wavelength that should avoid the excitation of Er^{3+} ion optical transitions.

4. Conclusions

Triple molybdate NCLM:$x$$Er^{3+}$,$y$$Yb^{3+}$ phosphors were successfully synthesized by the microwave sol–gel method. Well-crystallized particles formed after heat-treatment at 900 °C for 16 h showed a fine and homogeneous morphology with particle sizes of 2–3 μm. Under excitation at 980 nm, the UC doped particles exhibited a strong 525 nm emission band and a weak 550 nm emission band in the green region, corresponding to the $^2H_{11/2} \rightarrow {}^4I_{15/2}$ and $^4S_{3/2} \rightarrow {}^4I_{15/2}$ transitions, and a very weak 655 nm emission band in the red region, corresponding to the $^4F_{9/2} \rightarrow {}^4I_{15/2}$ transition. The preferable $Yb^{3+}:Er^{3+}$ ratio of 9 : 1 is controlled by the concentration quenching effect in Er^{3+} ions. The calculated slope value n indicated slopes of $n = 1.70$ and 1.68 for the green emission at 525 and 550 nm, respectively, and $n = 1.56$ for the red emission at 655 nm. The calculated chromaticity coordinates of the NCLM:$x$$Er^{3+}$,$y$$Yb^{3+}$ phosphors correspond to the yellowish-green sector in the CIE diagram.

Acknowledgements

This research was supported by the Basic Science Research Program of the National Research Foundation of Korea (NRF) funded by the Ministry of Education (2015-058813), by the Russian Foundation for Basic Research (15-52-53080) and by project no. 0358-2015-0012 of SB RAS Program no. II.2P. ASO and VVA are partially supported by the Ministry of Education and Science of the Russian Federation.

References

1 M. V. DaCosta, S. Doughan, Y. Han and U. J. Krull, Lanthanide upconversion nanoparticles and applications in bioassays and bioimaging: A review, *Anal. Chim. Acta*, 2014, **832**, 1–33.

2 Y. J. Chen, H. M. Zhu, Y. F. Lin, X. H. Gong, Z. D. Luo and Y. D. Huang, Efficient diode-pumped continuous-wave monolithic 1.9 μm micro-laser based on Tm^{3+}:$BaGd_2(MoO_4)_4$ cleaved plate, *Opt. Mater.*, 2013, **35**, 1422–1425.

3 C. Zhang, L. D. Sun, Y. W. Zhang and C. H. Yan, Rare earth upconversion nanophosphors: synthesis, functionalization and application as biolabels and energy transfer donors, *J. Rare Earths*, 2010, **28**, 807–819.

4 V. V. Atuchin, O. D. Chimitova, T. A. Gavrilova, M. S. Molokeev, S.-J. Kim, N. V. Surovtsev and B. G. Bazarov, Synthesis, structural and vibrational properties of microcrystalline $RbNd(MoO_4)_3$, *J. Cryst. Growth*, 2011, **318**, 683–686.

5 V. A. Morozov, A. Bertha, K. W. Meert, S. Van Rompaey, D. Batuk, G. T. Martinez, S. Van Aert, P. F. Smet, M. V. Raskina, D. Poelman, A. M. Abakumov and J. Hadermann, Incommensurate modulation and luminescence in the $CaGd_{2(1-x)}Eu_{2x}(MoO_4)_{4(1-y)}(WO_4)_{4y}$($0 \le x \le 1$, $0 \le y \le 1$) red phosphors, *Chem. Mater.*, 2013, **25**, 4387–4395.

6 P. L. Shi, Z. G. Xia, M. S. Molokeev and V. V. Atuchin, Crystal chemistry and luminescence properties of red-emitting $CsGd_{1-x}Eu_x(MoO_4)_2$ solid-solution phosphors, *Dalton Trans.*, 2014, **43**, 9669–9676.

7 C. S. Lim, A. Aleksandrovsky, M. Molokeev, A. Oreshonkov and V. Atuchin, The modulated structure and frequency upconversion properties of $CaLa_2(MoO_4)_4$:Ho^{3+}/Yb^{3+} phosphors prepared by microwave synthesis, *Phys. Chem. Chem. Phys.*, 2015, **17**, 19278–19287.

8 V. V. Atuchin, A. S. Aleksandrovsky, O. D. Chimitova, C.-P. Diao, T. A. Gavrilova, V. G. Kesler, M. S. Molokeev, A. S. Krylov, B. G. Bazarov, J. G. Bazarova and Z. S. Lin, Electronic structure of β-$RbSm(MoO_4)_2$ and chemical bonding in molybdates, *Dalton Trans.*, 2015, **44**, 1805–1815.

9 C. S. Lim, Highly modulated structure and upconversion photoluminescence properties of $PbGd_2(MoO_4)_4$:Er^{3+}/Yb^{3+}, *Mater. Res. Bull.*, 2016, **75**, 211–216.

10 O. D. Chimitova, V. V. Atuchin, B. G. Bazarov, M. S. Molokeev and Z. G. Bazarova, The formation and structural parameters of new double molybdates $RbLn(MoO_4)_2$ (Ln = Pr, Nd, Sm, Eu), *Proc. SPIE-Int. Soc. Opt. Eng.*, 2013, **8771**, 87711A.

11 C. F. Guo, H. K. Yang and J.-H. Jeong, Preparation and luminescent properties of phosphor $MGd_2(MoO_4)_4$: Eu^{3+} (M = Ca, Sr and Ba), *J. Lumin.*, 2010, **130**, 1390–1393.

12 J. Y. Sun, Y. J. Lan, Z. G. Xia and H. Y. Du, Sol–gel synthesis and green upconversion luminescence in $BaGd_2(MoO_4)_4$:Yb^{3+},Er^{3+} phosphors, *Opt. Mater.*, 2011, **33**, 576–581.

13 J. S. Liao, D. Zhou, B. Yang, R. Q. Liu, Q. Zhang and Q. H. Zhou, Sol–gel preparation and photoluminescence properties of $CaLa_2(MoO_4)_4$:Eu^{3+} phosphors, *J. Lumin.*, 2013, **134**, 533–538.

14 F. R. Chen, Z. G. Xia, M. S. Molokeev and X. P. Jing, Effects of composition modulation on the luminescence properties of Eu^{3+} doped $Li_{1-x}Ag_xLu(MoO_4)_2$ solid-solution phosphors, *Dalton Trans.*, 2015, **44**, 18078–18089.

15 C. S. Lim, Preparation of $CaLa_2(MoO_4)_4$:Er^{3+}/Yb^{3+} phosphors via the microwave-modified sol-gel route and the upconversion of their photoluminescence properties, *Mater. Res. Bull.*, 2014, **60**, 537–542.

16 C. S. Lim, Upconversion photoluminescence properties of $SrY_2(MoO_4)_4$:Er^{3+}/Yb^{3+} phosphors synthesized by a cyclic microwave-modified sol-gel method, *Infrared Phys. Technol.*, 2014, **67**, 371–376.

17 J. Y. Sun, W. Zhang, W. H. Zhang and H. Y. Du, Synthesis and two-color emission properties of $BaGd_2(MoO_4)_4$:Eu^{3+},Er^{3+},Yb^{3+} phosphors, *Mater. Res. Bull.*, 2012, **47**, 786–789.

18 J. F. Tang, C. H. Cheng, Y. J. Chen and Y. D. Huang, Yellow–green upconversion photoluminescence in Yb^{3+}, Ho^{3+} co-doped $NaLa(MoO_4)_2$ phosphor, *J. Alloys Compd.*, 2014, **609**, 268–273.

19 W. T. Zhang, J. F. Li, Y. L. Wang, J. P. Long and K. H. Qiu, Synthesis and luminescence properties of $NaLa(MoO_4)_{2-x}AG_x$:Eu^{3+} (AG = SO_4^{2-}, BO_3^{3-}) red phosphors for white light emitting diodes, *J. Alloys Compd.*, 2015, **635**, 16–20.

20 F. W. Mo, L. Zhou, Q. Pang, F. Z. Gong and Z. J. Liang, Potential red-emitting $NaGd(MO_4)_2$:R (M = W, Mo, R = Eu^{3+}, Sm^{3+}, Bi^{3+}) phosphors for white light emitting diodes applications, *Ceram. Int.*, 2012, **38**, 6289–6294.

21 G. H. Li, S. Lan, L. L. Li, M. M. Li, W. W. Bao, H. F. Zou, X. C. Xu and S. C. Gan, Tunable luminescence properties of $NaLa(MoO_4)_2$:Ce^{3+},Tb^{3+} phosphors for near UV-excited white light-emitting-diodes, *J. Alloys Compd.*, 2012, **513**, 145–149.

22 J. S. Liao, H. Z. Huang, H. Y. You, X. Qiu, Y. Li, B. Qiu and H.-R. Wen, Photoluminescence properties of $NaGd(MoO_4)_2$:Eu^{3+} nanophosphors prepared by sol–gel method, *Mater. Res. Bull.*, 2010, **45**, 1145–1149.

23 F.-B. Cao, L.-S. Li, Y.-W. Tian and X.-R. Wu, Sol–gel synthesis of red-emitting $[Na_{0.6}La_{0.8-x}Eu_x]_2(MoO_4)_3$ phosphors and improvement of its luminescent properties by the co-doping method, *Opt. Laser Technol.*, 2014, **55**, 6–10.

24 G. M. Kuz'micheva, D. A. Lis, K. A. Subbotin, V. B. Rybakov and E. V. Zharikov, Growth and structural X-ray investigations of scheelite-like single crystals Er, Ce:$NaLa(MoO_4)_2$ and Yb:$NaGd(WO_4)_2$, *J. Cryst. Growth*, 2005, **275**, e1835–e1842.

25 X. A. Lu, Z. N. You, J. F. Li, Z. J. Zhu, G. H. Jia, B. C. Wu and C. Y. Tu, Optical absorption and spectroscopic characteristics of Tm^{3+} ions doped $NaY(MoO_4)_2$ crystal, *J. Alloys Compd.*, 2008, **458**, 462–466.

26 X. Z. Li, Z. B. Lin, L. Z. Zhang and G. F. Wang, Growth, thermal and spectral properties of Nd^{3+}-doped $NaGd(MoO_4)_2$ crystal, *J. Cryst. Growth*, 2006, **290**, 670–673.

27 Y. K. Voron'ko, K. A. Subbotin, V. E. Shukshin, D. A. Lis, S. N. Ushakov, A. V. Popov and E. V. Zharikov, Growth and spectroscopic investigations of Yb^{3+}-doped $NaGd(MoO_4)_2$ and $NaLa(MoO_4)_2$ - new promising laser crystals, *Opt. Mater.*, 2009, **29**, 246–252.

28 H. Lin, X. H. Yan and X. F. Wang, Controllable synthesis and down-conversion properties of flower-like $NaY(MoO_4)_2$ microcrystals via polyvinylpyrrolidone-mediated, *J. Solid State Chem.*, 2013, **204**, 266–271.

29 G. H. Li, L. L. Li, M. M. Li, W. W. Bao, Y. H. Song, S. C. Gan, H. F. Zou and X. C. Xu, Hydrothermal synthesis and luminescent properties of $NaLa(MoO_4)_2$:Eu^{3+},Tb^{3+} phosphors, *J. Alloys Compd.*, 2013, **550**, 1–8.

30 Y. Huang, L. Q. Zhou, L. Yang and Z. W. Tang, Self-assembled 3D flower-like $NaY(MoO_4)_2$:Eu^{3+} microarchitectures: Hydrothermal synthesis, formation mechanism and luminescence properties, *Opt. Mater.*, 2011, **33**, 777–782.

31 L. L. Li, W. W. Zi, G. H. Li, S. Lan, G. J. Ji, S. C. Gan, H. F. Zou and X. C. Xu, Hydrothermal synthesis and luminescent properties of $NaLa(MoO_4)_2$:Dy^{3+} phosphor, *J. Solid State Chem.*, 2012, **191**, 175–180.

32 Y. Tian, B. J. Chen, B. N. Tian, J. S. Sun, X. P. Li, J. S. Zhang, L. H. Cheng, H. Y. Zhong, H. Zhong, Q. G. Meng and R. N. Hua, Ionic liquid-assisted hydrothermal synthesis of dendrite-like $NaY(MoO_4)_2$:Tb^{3+} phosphor, *Physica B*, 2012, **407**, 2556–2559.

33 J. C. Zhang, X. F. Wang, X. H. Zhang, X. D. Zhao, X. Y. Liu and L. P. Peng, Microwave synthesis of $NaLa(MoO_4)_2$ microcrystals and their near-infrared luminescent properties with lanthanide ion doping (Er^{3+}, Nd^{3+}, Yb^{3+}), *Inorg. Chem. Commun.*, 2011, **14**, 1723–1727.

34 S. W. Park, B. K. Moon, B. C. Choi, J. H. Jeong, J. S. Bae and K. H. Kim, Red photoluminescence of pulsed laser deposited Eu:$NaY(MoO_4)_2$ thin film phosphors on sapphire substrates, *Curr. Appl. Phys.*, 2012, **12**, S150–S155.

35 K. I. Rybakov, E. A. Olevsky and E. V. Krikun, Microwave sintering: Fundamentals and modeling, *J. Am. Ceram. Soc.*, 2013, **96**, 1003–1020.

36 H. J. Kitchen, S. R. Vallance, J. I. Kennedy, N. Tapia-Ruiz, L. Carassiti, A. Harrison, A. G. Whittaker, T. D. Drysdale, S. W. Kingman and D. H. Gregory, Modern microwave methods in solid-state inorganic materials chemistry: From fundamentals to manufacturing, *Chem. Rev.*, 2014, **114**, 1170–1206.

37 C. S. Lim, Cyclic MAM synthesis and upconversion photoluminescence properties of $CaMoO_4$:Er^{3+}/Yb^{3+} particles, *Mater. Res. Bull.*, 2012, **47**, 4220–4225.

38 C. S. Lim, Preparation of $PbLa_2(MoO_4)_2$:Er^{3+}/Yb^{3+} particles via microwave sol-gel route and upconversion photoluminescence properties, *Ceram. Int.*, 2015, **41**, 12464–12470.

39 C. S. Lim, V. Atuchin, A. Aleksandrovsky, M. Molokeev and A. Oreshonkov, Microwave sol-gel synthesis of $CaGd_2(MoO_4)_2$:Er^{3+}/Yb^{3+} phosphors and their upconversion photoluminescence properties, *J. Am. Ceram. Soc.*, 2015, **98**, 3223–3230.

40 *Bruker AXS TOPAS V4: General profile and structure analysis software for powder diffraction data – User's Manual*, Bruker AXS, Karlsruhe, Germany, 2008.

41 R. M. Hazen, L. W. Finger and J. W. E. Mariathasan, High-pressure crystal chemistry of scheelite-type tungstates and molybdates, *J. Phys. Chem. Solids*, 1985, **46**, 253–263.

42 S. B. Stevens, C. A. Morrison, T. H. Allik, A. L. Rheingold and B. S. Haggerty, $NaLa(MoO_4)_2$ as a laser host material, *Phys. Rev. B: Condens. Matter*, 1991, **43**, 7386–7394.

43 http://www.iucr.org/__data/iucr/cifdic_html/1/cif_core.dic/Cchemical_formula.html.

44 R. D. Shannon, Revised effective ionic radii and systematic studies of interatomic distances in halides and chalcogenides, *Acta Crystallogr., Sect. A: Cryst. Phys., Diffr., Theor. Gen. Cryst.*, 1976, **32**, 751–767.

45 V. V. Atuchin, V. G. Grossman, S. V. Adichtchev, N. V. Surovtsev, T. A. Gavrilova and B. G. Bazarov, Structural and vibrational properties of microcrystalline

$TlM(MoO_4)_2$ (M = Nd, Pr) molybdates, *Opt. Mater.*, 2012, **34**, 812–816.

46 V. V. Atuchin, A. S. Aleksandrovsky, O. D. Chimitova, A. S. Krylov, M. S. Molokeev, B. G. Bazarov, J. G. Bazarova and Z. Xia, Synthesis and spectroscopic properties of multiferroic β′-$Tb_2(MoO_4)_3$, *Opt. Mater.*, 2014, **36**, 1631–1635.

47 V. V. Atuchin, A. S. Aleksandrovsky, O. D. Chimitova, T. A. Gavrilova, A. S. Krylov, M. S. Molokeev, A. S. Oreshonkov, B. G. Bazarov and J. G. Bazarova, Synthesis and spectroscopic properties of monoclinic α-$Eu_2(MoO_4)_3$, *J. Phys. Chem.*, 2014, **C 118**, 15404–15411.

48 V. V. Atuchin, T. A. Gavrilova, J.-C. Grivel and V. G. Kesler, Electronic structure of layered titanate $Nd_2Ti_2O_7$, *Surf. Sci.*, 2008, **602**, 3095–3099.

49 V. V. Atuchin, S. V. Adichtchev, B. G. Bazarov, Zh. G. Bazarova, T. A. Gavrilova, V. G. Grossman, V. G. Kesler, G. S. Meng, Z. S. Lin and N. V. Surovtsev, Electronic structure and vibrational properties of $KRbAl_2B_2O_7$, *Mater. Res. Bull.*, 2013, **48**, 929–934.

50 V. Atuchin, L. Zhu, S. H. Lee, D. H. Kim and C. S. Lim, Microwave-assisted solvothermal synthesis of $Sr_3V_2O_8$ nanoparticles and their spectroscopic properties, *Asian J. Chem.*, 2014, **26**(5), 1290–1292.

51 F. Auzel, G. Baldacchini, L. Laversenne and G. Boulon, Radiation trapping and self-quenching analysis in Yb^{3+}, Er^{3+}, and Ho^{3+} doped Y_2O_3, *Opt. Mater.*, 2003, **24**, 103–109.

52 M. Pollnau, D. R. Gamelin, S. R. Lüthi and H. U. Güdel, Power dependece of upconversion luminescence in lanthanide and transition-metal-ion systems, *Phys. Rev. B: Condens. Matter*, 2000, **61**, 3337–3346.

53 H. Y. Du, Y. J. Lan, Z. G. Xia and J. Y. Sun, Synthesis and upconversion luminescence properties of Yb^{3+}/Er^{3+} codoped $BaGd_2(MoO_4)_4$ powder, *Mater. Res. Bull.*, 2009, **44**, 1660–1662.

54 B. Li, B. Joshi, Y. K. Kshetri, R. Adhikari, R. Narro-Gracia and S. W. Lee, Upconversion luminescence properties of Er^{3+}/Yb^{3+} in transparent a-Sialon ceramics, *Opt. Mater.*, 2015, **39**, 239–246.

55 J. H. Chung, J.-I. Lee, S.-L. Ryu and J. H. Ryu, Visible green upconversion luminescence of $Er^{3+}/Yb^{3+}/Li^{+}$ co-doped $CaWO_4$ particles, *Ceram. Int.*, 2013, **39**, S369–S372.

56 J. Castañeda, M. A. Meneses-Nava, O. Barbosa-García, E. de la Rosa-Cruz and J. F. Mosiño, The red emission in two and three steps up-conversion process in a doped erbium SiO_2–TiO_2 sol–gel powder, *J. Lumin.*, 2003, **102–103**, 504–509.

57 E. Sarantopoulou, C. Raptis, S. Ves, D. Christofilos and G. A. Kourouklis, Temperature and pressure dependence of Raman-active phonons of $CaMoO_4$: an anharmonicity study, *J. Phys.: Condens. Matter*, 2002, **14**, 8925–8938.

58 P. G. Zverev, Vibronic relaxation of Raman modes in $CaMoO_4$ and $PbMoO_4$ molecular ionic crystals, *Phys. Status Solidi C*, 2004, **1**, 3101–3105.

59 M. B. Smirnov and V. Yu. Kazimirov, *LADY: software for lattice dynamics simulations*, JINR Communications, 2001, E 14-2001-159.

60 I. F. Chang and S. S. Mitra, Application of a modified random-element-isodisplacement model to long-wavelength optic phonons of mixed crystals, *Phys. Rev.*, 1968, **172**, 924–933.

61 A. N. Vtyurin, A. S. Krylov, S. N. Krylova, S. V. Goryainov, V. N. Voronov and A. S. Oreshonkov, Hydrostatic pressure-induced phase transitions in Rb_2KInF_6 and Rb_2KScF_6 crystals: Raman spectra and lattice dynamics simulations, *Ferroelectrics*, 2012, **440**, 100–104.

62 Y. V. Gerasimova, A. S. Oreshonkov, A. N. Vtyurin, A. A. Ivanenko, L. I. Isaenko, A. A. Ershov and E. I. Pogoreltsev, Infrared absorption investigation of the role of octahedral groups upon the phase transition in the $Rb_2KMoO_3F_3$ crystal, *Phys. Solid State*, 2013, **55**, 2331–2334.

63 A. S. Krylov, A. N. Vtyurin, A. S. Oreshonkov, V. N. Voronov and S. N. Krylova, Structural transformations in a single-crystal Rb_2NaYF_6: Raman scattering study, *J. Raman Spectrosc.*, 2013, **44**, 763–769.

64 Z. G. Xia, M. S. Molokeev, A. S. Oreshonkov, V. V. Atuchin, R.-S. Liu and C. Dong, Crystal and local structure refinement in $Ca_2Al_3O_6F$ explored by X-ray diffraction and Raman spectroscopy, *Phys. Chem. Chem. Phys.*, 2014, **16**, 5952–5957.

65 A. A. Savina, V. V. Atuchin, S. F. Solodovnikov, Z. A. Solodovnikova, A. S. Krylov, E. A. Maximovskiy, M. S. Molokeev, A. S. Oreshonkov, A. M. Pugachev and E. G. Khaikina, Synthesis, structural and spectroscopic properties of acentric triple molybdate $Cs_2NaBi(MoO_4)_3$, *J. Solid State Chem.*, 2015, **225**, 53–58.

66 C. S. Lim, A. Aleksandrovsky, M. Molokeev, A. Oreshonkov and V. Atuchin, Microwave sol-gel synthesis and upconversion photoluminescence properties of $CaGd_2(WO_4)_4$:Er^{3+}/Yb^{3+} phosphors with incommensurately modulated structure, *J. Solid State Chem.*, 2015, **228**, 160–166.

67 R. Fletcher, *Practical Methods of Optimization*, Wiley, Chichester *etc.*, 2nd edn, 1987.

68 A. Senyshyn, H. Kraus, V. B. Mikhailik and V. Yakovyna, Lattice dynamics and thermal properties of $CaWO_4$, *Phys. Rev. B: Condens. Matter*, 2004, **70**, 214306.

69 A. Senyshyn, H. Kraus, V. B. Mikhailik, L. Vasylechko and M. Knapp, Thermal properties of $CaMoO_4$: Lattice dynamics and synchrotron powder diffraction studies, *Phys. Rev. B: Condens. Matter*, 2006, **73**, 014104.

70 F. D. Hardcastle and I. E. Wachs, Determination of molybdenum-oxygen bond distances and bond orders by Raman spectroscopy, *J. Raman Spectrosc.*, 1990, **21**, 683–691.

71 K. Nakamoto, *Infrared and Raman Spectra of Inorganic and Coordination Compounds*, Wiley, New York *etc.*, 6th edn, 2009.